BRAIN
ORIGINAL ARTICLE

Blockage of STAT3 during epileptogenesis prevents GABAergic loss and imprinting of the epileptic state

Soraya Martín-Suárez,[1,†] Jesús María Cortes[1,2,3] and Paolo Bonifazi[1,2]

[†]Present address: Achucarro Basque Center for Neuroscience. Edificio Sede 3p. Barrio Sarriena s/n, 48940 Leioa, Spain.

Epilepsy, characterized by recurrent unprovoked seizures resulting from a wide variety of causes, is one of the world's most prominent neurological disabilities. Seizures, which are an expression of neuronal network dysfunction, occur in a positive feedback loop of concomitant factors, including neuro-inflammatory responses, where seizures generate more seizures. Among other pathways involved in inflammatory responses, the JAK/STAT signalling pathway has been proposed to participate in epilepsy.

Here, we tested an *in vitro* model of temporal lobe epilepsy, with the hypothesis that acute blockage of STAT3-phosphorylation during epileptogenesis would prevent structural damage in the hippocampal circuitry and the imprinting of both neural epileptic activity and inflammatory glial states. We performed calcium imaging of spontaneous circuit dynamics in organotypic hippocampal slices previously exposed to epileptogenic conditions through the blockage of GABAergic synaptic transmission.

Epileptogenic conditions lead to epileptic dynamics imprinted on circuits in terms of increased neuronal firing and circuit synchronization, increased correlated activity in neuronal pairs and decreased complexity in synchronization patterns. Acute blockage of the STAT3-phosphorylation during epileptogenesis prevented the imprinting of epileptic activity patterns, general cell loss, loss of GABAergic neurons and the persistence of reactive glial states. This work provides mechanistic evidence that blocking the STAT3 signalling pathway during epileptogenesis can prevent patho-topological persistent reorganization of neuro-glial circuits.

1 Computational Neuroimaging Laboratory, Biocruces-Bizkaia Health Research Institute, Bizkaia 48903, Spain
2 IKERBASQUE: The Basque Foundation for Science, Bilbao 48009, Spain
3 Department of Cell Biology and Histology, University of the Basque Country (UPV/EHU), Leioa 48940, Spain

Correspondence to: Paolo Bonifazi
Computational Neuroimaging Laboratory
Biocruces-Bizkaia Health Research
Institute Cruces Plaza, Barakaldo, Bizkaia 48903, Spain
E-mail: paol.bonifazi@gmail.com

Correspondence may also be addressed to: Soraya Martín-Suárez
Laboratory of Neural Stem Cells and Neurogenesis; Science Park of the UPV/EHU
Sede Building, 3rd floor, Barrio Sarriena, s/n, Leioa E-48940, Spain
E-mail: soraya.martin@achucarro.org

Keywords: calcium imaging; epilepsy; STAT3; gliosis; GABA

Received August 22, 2022. Revised January 04, 2023. Accepted February 03, 2023. Advance access publication February 24, 2023

Introduction

Epilepsy is a neurological disorder characterized by chronic aberrant patterns of cerebral activity, i.e. seizures, which appear in conjunction with other symptoms such as convulsions, loss of consciousness and mental absence. Typically, once they have appeared, epileptic patterns remain imprinted in the brain, and ictal activity reappears chronically, possibly developing and scaling up symptoms with additional dysfunction.[1–4] The relationship between causes, prognosis and symptomatology is broad, complex and not fully understood.[5] As a result, not all epileptic patients respond equally to the same drugs.[6,7] Antiepileptic drugs can work via different mechanisms and often are aimed at preventing hyper-excitable brain conditions that provide a fertile substrate for ictal patterns to appear and uncontrollably spread to the rest of the brain.[8,9]

The epileptogenic process, leading to the final imprinting of an epileptic brain, has been hypothesized to be a positive feedback loop in which seizures lead to more seizures through complex interactions that involve, among others, neuronal death, gliosis, emergence of aberrant connectivity, hyper-excitation and neuroinflammation.[10] In the case of temporal lobe epilepsy (TLE), the most prevalent form of epilepsy, the circuit originating the seizures is located in the temporal region of the brain, specifically the hippocampus. Although the triggers that cause the hippocampus to become epileptogenic are not always known, and drugs are not always effective as treatment, sometimes its surgical removal can lead to the disappearance of the seizures, confirming its key role in the generation of ictal activity.[11]

Understanding the mechanisms underlying epileptogenesis, i.e. what turns a functional circuit into an epileptic one capable of generating ictal patterns of activity, is still a major open question: the key to developing new effective treatments for epilepsy.

In our study, we aimed to provide a clearer link between gliosis (an initial marker of the neuro-glial inflammatory response) and epileptogenesis. In the last few years, clinical studies and experimental findings have confirmed that inflammatory pathways are implicated in epilepsy. Although several signalling pathways have been suggested to participate in the development and progression of epilepsy, in this study we focused on the JAK/STAT signalling pathway and, in particular, the STAT3 transcription factor. This pathway is involved in several processes such as cellular proliferation, differentiation, neuron survival, death and synaptic plasticity.[12–14] The induction of epilepsy leads to activation of STAT3[15]; therefore, it has been hypothesized that its inhibition could reduce neuronal damage and the progression of epilepsy. WP1066, which inhibits the STAT3 pathway, has been reported to reduce seizure severity and the progression of early epileptogenesis in a mouse model of epilepsy,[16] but the mechanisms of these effects are far from being understood.

In our study, we hypothesized that the acute blockage of STAT3 in the presence of pro-epileptic conditions could attenuate the damage induced by the reactive gliosis response on brain circuits, preventing the manifestation of epileptic activity[16] along with cell loss.

Our results lay in the longitudinal monitoring of the activity of circuits previously exposed to epileptogenic hyper-excitation by simultaneous blockage of GABAergic synaptic transmission and STAT3 signalling. In particular, we show that affecting the JAK/STAT pathway prevents the future appearance of hypersynchronized patterns of activity, cell loss, depletion of inhibitory cells and persistence of gliosis (a main marker for neuro-glial inflammatory states). Our study provides strong support that acute treatments affecting reactive gliosis can prevent patho-topological reorganizations that lead to the imprinting of epileptic dynamics.

Materials and methods

Hippocampal organotypic slice cultures

The preparation of slice cultures was carried out as described by Obiega *et al.*[17] In brief, post-natal Day (P)5–7 wild-type pups were decapitated and the brains extracted and placed in cold dissection medium [96% HBSS, 2% HEPES, 1% penicillin/streptomycin, 0.7% glucose (2.5 M) and 0.3% of NaOH (0.5 M)]. Both hippocampi were dissected out and cut into 300 μm slices using a vibratome. Both hippocampi were cut in cold artificial CSF (195 mM sucrose; 2.5 mM KCl; 1.25 mM NaH_2PO_4; 28 mM $NaHCO_3$; 0.5 mM $CaCl_2$; 1 mM L-ascorbic acid/Na-ascorbate; 3 mM pyruvic acid/Na-pyruvate; 7 mM glucose; 7 mM $MgCl_2$ in MiliQ) bubbled with 5% CO_2.[18] After slicing, the slices were transferred to 0.4 μm culture plate inserts (Millipore, PICM01250). The membranes were placed in 24-well plates, each well containing 250 μl of culture medium. The medium consisted of 50% Minimum Essential Medium supplemented with 2% B27, 25% horse serum, 2% Glutamax, 0.5% penicillin/streptomycin, 0.5% $NaHCO_3$, 0.5% glucose (2.5 M), 0.8% sucrose (2.5 M) and 18% HBSS. Slices were incubated at 37°C and 5% CO_2. The medum was changed on the first day after doing the culture and every 2 days afterwards. Slices were kept in culture for 7 days before changing to fresh culture medium without B27.[18,19]

Epilepsy was induced by the addition of the $GABA_A$ receptor inhibitor picrotoxin (PTX; 100 μM). PTX, vehicle or the inhibitor of the STAT3 pathway, WP1066 (1.25 μM), was added with serum-free media for 3 days. These results are shown in Supplementary Fig. 1A and B. As per the results in Supplementary Fig. 2A and B, it was added for 1 day starting at 12 days *in vitro* (DIV). During the induction of epilepsy, the medium was replaced every day, adding fresh serum-free media and PTX/vehicle and/or WP1066.

To evaluate the role of glutamatergic synaptic transmission on the dynamics of the induced circuits following exposure to epileptogenic conditions (i.e. 3 days after exposure to PTX), we blocked AMPA/kainate and NMDA receptors simultaneously by applying CNQX (6-cyano-7-nitroquinoxaline-2,3-dione) (20 μM) and D-AP5 (D-2-amino-5-phosphonopentanoate) (10 μM), respectively.

Calcium imaging set-up and recording

In preparation for calcium imaging, slices were infected with the calcium indicator AAV1.SYN.Gcamp6f.WPRE.SV40[20] at 1 week after slicing. Twenty-four hours after infection, the medium was changed. Calcium imaging was performed using a 20× objective on an inverted microscope (Zeiss Axio Observer.Z1 Apotome.2) for living cell imaging, equipped with an AxioCam MRc camera, a chamber for CO_2 and temperature control for maintaining the same conditions as in the cellular incubator. For imaging, the 24-well plates containing slices from the same animal donor under the four different conditions [control (CNT), Control + WP1066 (CNT-WP), PTX, PTX-WP)] were transferred to the microscope. The activity of each slice was then imaged for a duration of 20 min. All slices were imaged consecutively, and we did not follow any predefined sequence in the order of the slice being imaged in relation to the slice group. The plates were left open to maintain the culture conditions and avoid any disturbance.

For the analysis of CNQX (6-cyano-7-nitroquinoxaline-2,3-dione)-D-AP5(DL-2-amino-5-phosphonopentanoic acid), the slices were first imaged for 10 min to obtain the basal activity, then CNQX or D-AP5 were added to the media, and after 30 min of incubation under controlled conditions (37°C and 5% CO_2), the activity of each slice was again imaged for another 15 min.

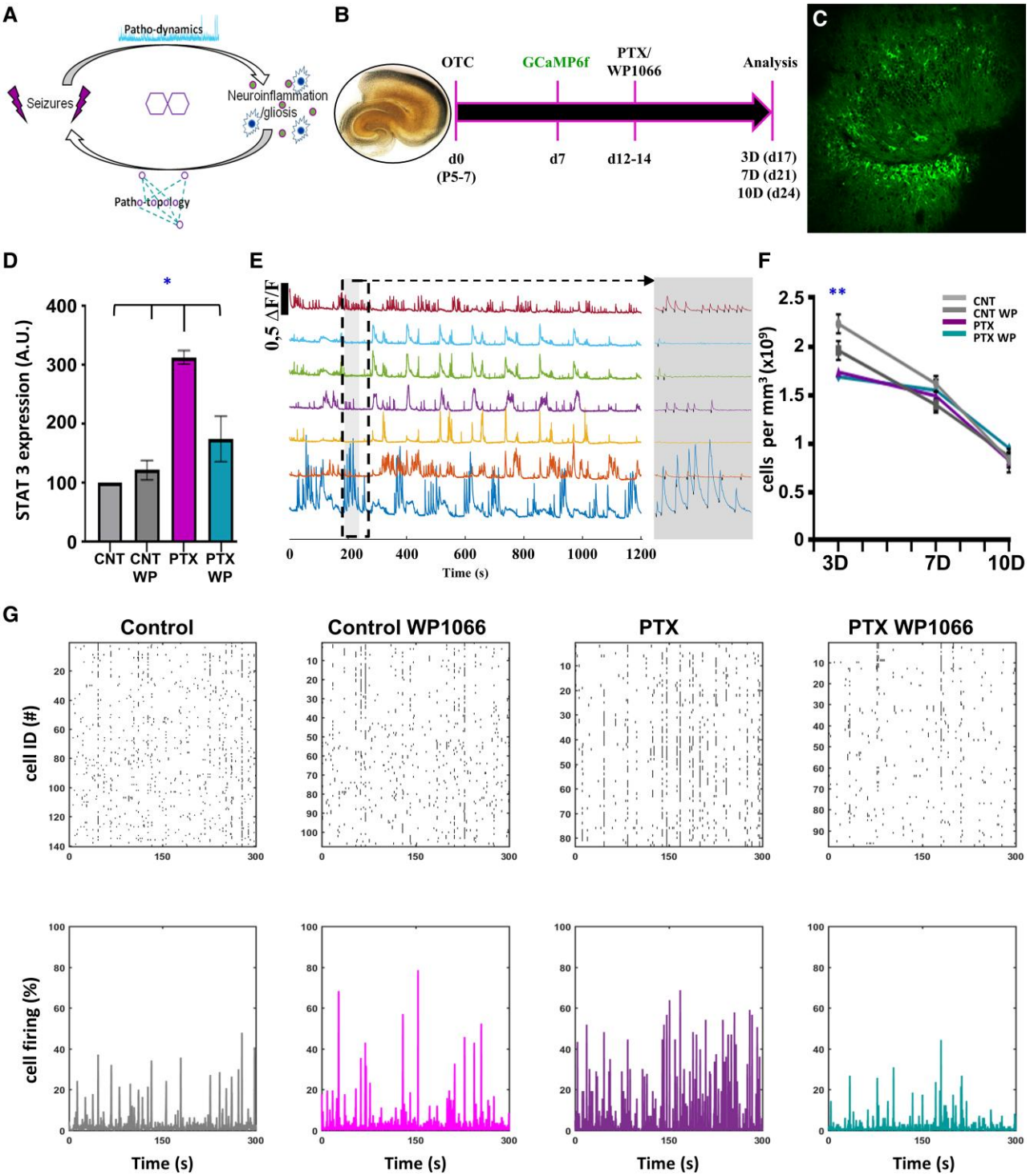

Figure 1 Experimental model, longitudinal calcium imaging and immunostaining. (**A**) Scheme of the positive feedback loop mechanism where seizures lead to more seizures through complex interactions that involve gliosis and neuroinflammation ultimately leading to patho-topological organization of the neuro-glial circuit. (**B**) Scheme of the experimental procedure. The organotypic slices (OTC) were extracted at P5–7 (Day 0, d0) and cultured. After 7 days (Day 7, d7), slices were infected for the expression of the GCaMP6f. From Day 12 (d12) to Day 14 (d14), slices were exposed to PTX and/or WP1066. Imaging and immunostaining were performed 3, 7 and 10 days afterwards [i.e. at Days 17 (d17), 21 (d21) and 24 (d24); we refer to them, respectively, as 3D, 7D and 10D]. (**C**) Representative image acquired at ×10 magnification of the cells expressing the calcium sensor at d17. Note that imaging of the neurons was performed in a quarter of the field shown, corresponding with the GCL region. (**D**) Quantification of STAT3 levels by quantitative PCR with reverse transcription on the third day of PTX exposure. (**E**) Representative calcium traces of seven neurons from a control slice at d17 with a zoomed-in visualization (grey shaded) of the calcium traces and spike onsets highlighted with black markers. (**F**) Health of the circuits as assessed by the density of live cells per mm^3. (**G**) Representative raster plots (*top*) showing the calcium spike onsets of each cell over time in the four experimental groups at d17. The percentage of active cells per frame is plotted at the *bottom*.

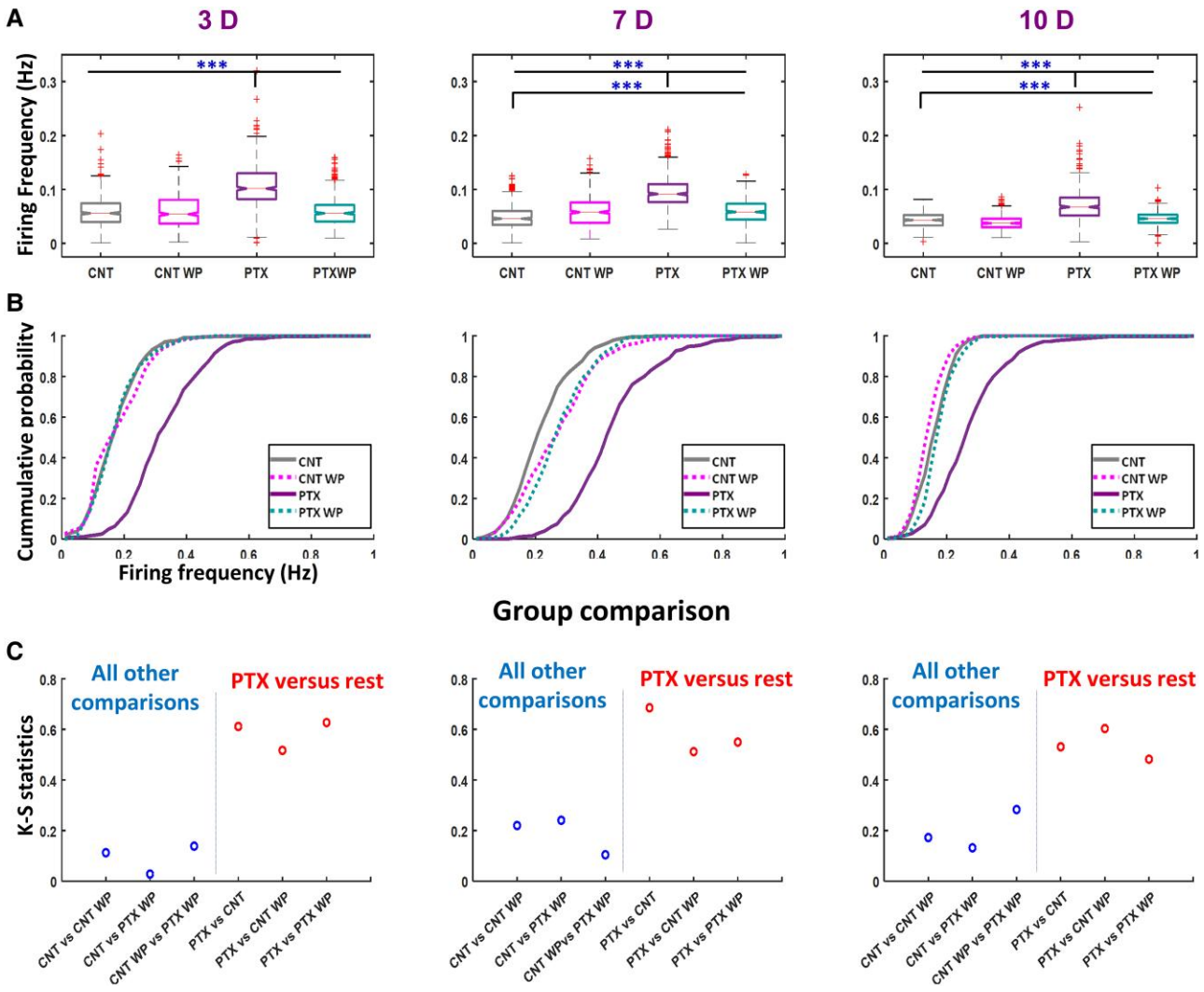

Figure 2 Single-neuron level: frequency of calcium events. For each cell, the average inverse of the intervals between consecutive calcium spikes is considered to be the firing rate. From *left* to *right*: Results from slices at 3D, 7D and 10D are shown. (**A**) Pooled values at 3–7 and 10D across all slices show the median (horizontal line) 25th–75th percentile limits, bottom to top range values and outliers (marked by red asterisks). (**B**) Cumulative distributions were obtained as an average across slices belonging to the same condition. Fifty identical equally sized intervals were chosen within the minimum–maximum range of the variable across all groups. (**C**) The maximum difference between cumulative distributions shown in **B** (KS–S) for all group comparisons. *Right*: Dots highlight the comparison in the PTX group versus all other groups. *Left*: Dots represent all other comparisons. Significant data are denoted with asterisks: $^{*}P < 0.05$; $^{**}P < 0.01$; $^{***}P < 0.001$.

Analysis of calcium imaging and circuit dynamics

Neuronal cell body segmentation was performed as described by Kenner *et al.*[21] Briefly, the maximum value of each pixel across all calcium images acquired for a given slice was used to reconstruct the image template and to segment the contours of the neuronal cells using the custom-made software HIPPO. For each frame, the average value of the pixels within a cell contour was calculated, and for each cell, a calcium time series was then constructed across all frames. The time series were first high-pass filtered above 0.05 Hz to remove slow fluctuations and baseline changes, and the traces were then deconvolved using the MATLAB function 'deconvolveCa' with default options, as derived and described by Friedrich *et al.*[22] The onsets of the calcium events were extracted from the deconvolved calcium signal with start and end points set by the respective thresholds of 0.05 and 0.04 $\Delta F/F$ (i.e. with a ratio of 1.25). The automatic detection of calcium spikes was later visually inspected for each cell. When the event detection was considered faulty, the starting and ending thresholds of a given calcium trace were adjusted manually, always keeping, respectively, a ratio of 1.25 between them. A binary time series representing the calcium activity in each frame was first reconstructed for each cell, where the 'ones' marked the onset of calcium spikes. For each cell, the interval between two consecutive onsets was used as the instantaneous firing rate (IF). To calculate the firing correlation in each neuronal pair, the binary time series were smoothed with a Gaussian moving average using the MATLAB 'smoothdata' function with a window length of four points, and the correlation C_{ij} was calculated as:

$$C_{ij} = \frac{1}{\| x_i \| \; \| x_j \|} \sum_{t=1}^{T} x_i(t) x_j(t) \qquad (1)$$

where $x_i(t)$ and $x_j(t)$ represent the time series of the neuronal pair (i, j), T the total number of frames (typically about 4800 for a 20 min recording) and the symbol $\|$ represents the norm of a vector [i.e. the time series $x_i(t)$ and $x_j(t)$].

Only for assessing global synchronization were the binary time series $x_i(t)$ smoothed with a different window length of 20, represented by $s_i(t)$, to address the dynamics emerging over larger time windows compared to the one from the neuronal pair. We calculated the global synchronization index at time t, $GSI(t)$, by summing over all network smoothed activity:

$$GSI(t) = \sum_{i=1}^{n} s_i(t) \quad (2)$$

where n is the total number of imaged neurons. Network synchronizations (NSs) exceeding a threshold of chance level with $P < 0.05$, were identified by GSI, as calculated from 1000 reshuffled network dynamics in which single-neuron time series were randomized, while keeping the same inter-event distribution in each neuron.

To each NS was assigned the timestamp of the peak of the corresponding GSI. All the cells recruited within a time window of seven frames around the GSI peak were considered to be participating in the NS. The size of a NS event was calculated as the percentage of cells participating in a given NS out of the total number n of imaged neurons in the circuit. The instantaneous frequency of the NS in a given circuit was calculated as the inverse of the intervals (in seconds) between consecutive NSs. The similarity between two NSs was calculated as the cosine between the two binary vectors A and B:

$$S_{AB} = \frac{1}{\| A \| \ \| B \|} \sum_{i=1}^{n} A_i B_i \quad (3)$$

where the vector components i are set to 1 if the neuron i is participating in the corresponding NS and 0 otherwise.

Table 1 shows for each group and day of recording, and for each slice, the imaged neurons per slice (ImN) and the number of NSs that occurred within the 20 min duration of the recordings.

Immunostaining protocol

At the end of the calcium imaging sessions, slices were washed with PBS and fixed with 4% paraformaldehyde for 30 min at room temperature. Immunohistochemical techniques were performed as described previously.[23,24] Slices were incubated with blocking and permeabilization solution containing 0.25% Triton-X100 and 3% bovine serum albumin in PBS for 3 h at room temperature. They were then incubated overnight with the primary antibodies (diluted in the same solution) at 4°C. After washing with PBS, the sections were incubated with fluorochrome-conjugated secondary antibodies diluted in the permeabilization and blocking solution for 3 h at room temperature. After washing with PBS, the sections were mounted on slides with Dako fluorescent mounting medium (Agilent-Dako S3023). The following primary antibodies were used: goat α-glial fibrillary acidic protein (GFAP) (Abcam Ab53554, 1:1000); rabbit α-Iba 1 (Wako 19- 19741, 1:1000); mouse α-NeuN (MerkMillipore, MAB377, 1:1000); rabbit α-GABA (GeneTex GTX125988, 1:1000); and rabbit α-GAD (Sigma-Aldrich G5163). The secondary antibodies (ThermoFisher Scientific; 1:1000), were: donkey α-rabbit Alexa Fluor 568 (A10043); donkey α-mouse Alexa Fluor 647 (A-31571); goat α-rabbit Alexa Fluor 488 (A-11034); and donkey α-goat Alexa Fluor 488 (A-21084). 4′,6-diamidino-2-phenylindole (DAPI, Sigma-Aldrich D9542) was used for staining.

Image capture and analysis of immunostaining

All fluorescence images were collected with a Leica Stellaris 5 (Leica) microscope and LASAF software. Images were exported as .tiff files and adjusted for brightness and background using Adobe Photoshop ('levels' tool). All images shown are projections, from z-stacks of ~5 µm thickness.

GABA/GAD quantification

Quantitative analysis of cell populations was performed by design-based (assumption free, unbiased) stereology using a modified optical fractionator-sampling scheme.[23,24] All the quantifications regarding the GABAergic cell population were normalized to the number of NeuN+ cells (all neurons) in each slice. Therefore, we quantified the proportion of GABAergic cells within the total neuronal population.

Astrogliosis/microgliosis

The area occupied by astrocytes was measured in the slices using the open-source FIJI (ImageJ). $GFAP^+$-cells were selected in z-stacks using the 'Threshold' tool to outline the pixels of the image labelled with GFAP. The 'Measure' tool was used to calculate the percentage area occupied by the staining in the image that had been highlighted using the threshold.[25] Both measures were calculated from at least five z-stacks from a minimum of three hippocampal slices.

Apoptosis

Apoptosis was quantified as previously described.[25] The number of pyknotic/karyorrhectic (condensed/fragmented DNA) nuclei were quantified in the region of the granule cell layer (GCL) + subgranular zone (SGZ).

Statistical analysis

GraphPad Prism (v.6 for Windows) was used for statistical analysis in Figs 5 and 6. One-way ANOVA was performed in all cases to compare data from the CNT, CNT-WP, PTX and PTX-WP groups in all the experiments. Error bars represent mean + standard error of the mean (SEM). Dots show individual data points. To confirm the effect of the analysis, Student's t-test was carried out. Results are expressed as means ± SEM. Significant data are denoted with asterisks as follows: $^*P < 0.05$; $^{**}P < 0.01$; $^{***}P < 0.001$.

MATLAB was used for the statistical analysis of the following variables quantifying networks' dynamics: single-neuron firing rate, neuronal pair correlation, NS (size and frequency) and synchronization similarity.

The analysis was performed similarly in Figs 2A, 3A and 5A, Fig. 4B and C and Supplementary Figs 1 and 2, using pooled datasets. Specifically, given a variable, all the data obtained from different slices belonging to a given experimental group (CNT, CNT-WP, PTX, PTX-WP) and day of experiment [Day 3 (3D), Day 7 (7D) and Day 10 (10D)] were pooled. *Post hoc* statistical differences between groups were assessed using the Kruskall–Wallis test for non-parametric group comparisons with corresponding P-values for each pair of groups. Corresponding plots represent medians, 25–75% percentile limits, smallest-highest values and outliers for each group.

Figs 2B, 3B and 5B and Fig. 4D and E represent the cumulative distributions obtained as averages across slices for a given

Table 1 The total number of slices imaged, the imaged neurons per slice (ImN) and the number of circuit synchronizations (NS) that occurred during the 20 min recordings for each group and day of recording

Condition	Control			Control WP			PTX			PTX-WP		
Day	Slice	ImN	NS	Slice	ImN	NS	Slice	ImN	NS	Slice	ImN	NS
3	1	70	31	1	71	56	1	83	94	1	56	36
	2	77	80	2	66	58	2	105	55	2	97	56
	3	163	75	3	150	44	3	84	67	3	105	53
	4	140	72	4	107	57	4	113	94	4	112	96
	5	135	54	5	109	67	5	59	61	5	79	53
		–	–	–	–	–	6	95	168	–	–	–
7	1	99	55	1	72	41	1	70	94	1	139	87
	2	100	74	2	124	80	2	92	94	2	90	77
	3	105	64	3	84	54	3	96	63	3	98	74
	4	58	43	4	103	39	4	100	72	4	102	57
	5	75	38	5	84	53	5	107	74	5	101	51
10	1	73	19	1	113	73	1	77	65	1	101	88
	2	107	24	2	128	102	2	66	71	2	105	90
	3	101	42	3	94	102	3	102	127	3	119	97
	4	125	37	4	88	48	4	90	95	–	–	–
	5	88	46	5	104	83	5	97	64	–	–	–

experimental group and day of recording. Specifically, the range of the considered variable (from the smallest to the highest value) was equally divided into 50 intervals. For each slice, the cumulative distribution of the variable was calculated on such intervals. The average cumulative distribution across slices was then calculated and plotted.

Figs 2C, 3C and 5C and Fig. 4F and G plot the Kolmogorov–Smirnov statistics (KS–S) as a measure of distance between two experimental groups. Given a pair of experimental groups (out of CNT, CNT-WP, PTX and PTX-WP), the KS–S was calculated as the maximum difference between the corresponding cumulative distributions on each interval of the variable considered.[26]

Data availability

The data that support the findings of this study are available from the corresponding author, upon reasonable request.

Results

Testing epileptiform activity by monitoring longitudinally neuronal firing in organotypic slices

To assess the impact of inhibiting STAT3 signalling pathway during epileptogenesis, we studied *in vitro* hippocampal organotypic slices generated at P5–7 and cultured for at least 17 days (see Fig. 1A and B).

As a model of epileptogenesis, we exposed the circuits to hyper-excitation transitorily, by blocking GABAergic transmission with picrotoxin (PTX), an antagonist of the GABA-A receptor. STAT3 pathway blockage was performed using WP1066, which inhibits the transcription of the STAT3 gene.[16] We designed four experimental groups: (i) the control condition (CNT group), in which cultured slices were never exposed to epileptogenesis or STAT3 inhibition; (ii) the epileptogenic condition (PTX group), in which cultured slices underwent suppression of GABAergic transmission in extracellular presence of PTX (100 µM) from DIV12–14; (iii) the epileptogenic and inhibited-STAT3 condition (PTX-WP group), in which slices underwent suppression of GABAergic transmission as in the PTX group with simultaneous extracellular application of the STAT3 inhibitor WP-1066 (1.25 µM); and (iv) the control under inhibited-STAT3 condition (CNT; CNT-WP group), in which slices were exposed to WP1066 (1.25 µM) from DIV12–14. The slices obtained from the same animal (batch) were separated to cover the four different experimental conditions, cultured on the same multi-well plate and imaged on the same DIV (see the 'Materials and methods' section). The effective need for prolonged exposure (3 days) to GABAergic synaptic blockers to induce a sufficiently long epileptogenic time window, leading to an impact on the dynamical states of the slices, was preliminarily verified (Supplementary Fig. 1A and B) in relation to single-neuron and global circuit dynamics as described below in the corresponding 'Results' sections.

To monitor longitudinally the activity of circuits, we expressed GCaMP6f only in neurons (with viral infection at 7 DIV under the hSyn promoter, see the 'Materials and methods' section; Fig. 1B) and performed calcium imaging around the GCL (Fig. 1C) at 17, 21 and 24 DIV (which corresponded to 3, 7 and 10 days following the application of PTX/WP1066; Fig. 1B). The blockage of STAT3 expression using WP1066 was first checked by quantifying using quantitative PCR with reverse transcription of the mRNA levels of STAT3 on the third day of PTX exposure, under the different conditions (Fig. 1D). The treatment with PTX increased the expression of STAT3, whereas it was prevented by concomitant application of WP1066. The spontaneous circuit dynamics were monitored simultaneously in several dozen neurons over 20 min, while fully preserving the culturing conditions. Following semi-automated cell contour segmentation and detection of calcium spikes, the onsets of calcium events were extracted from each neuronal trace to reconstruct the circuit dynamics from single-neuron firing properties to pair and ensemble synchronizations (Fig. 1E–G). In addition, at 3D, 10D and 10D, slices were stained for the immunochemical characterization of the glial neuro-inflammatory state of cellular alterations (i.e. counting alive/apoptotic cells and GABAergic cell density in the GCL; Figs 1F, 6 and 7). The density of live cells was used to monitor the health of the organotypic cultures (Fig. 1F). As expected, there was a progressive decrease in cell density with time in culture.[27]

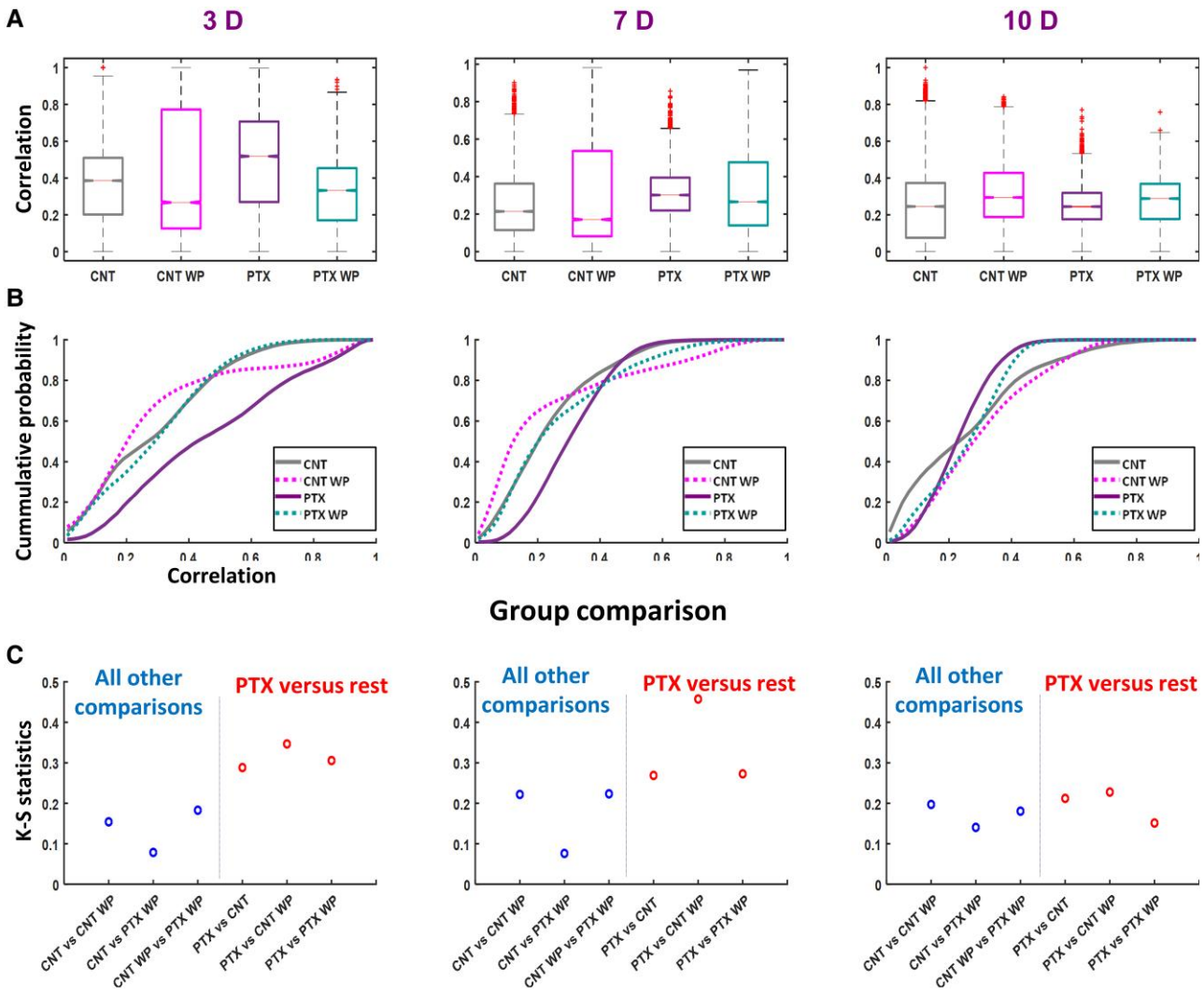

Figure 3 Pair-wise level: firing correlation in neuronal pairs. (**A**) Pooled values at 3–7 and 10D across all slices of the firing correlation show the median (horizontal line) 25th–75th percentile limits, bottom to top range values and outliers (marked by red asterisks). (**B**) Cumulative distributions obtained as averages across slices belonging to the same conditions. Fifty identical equally sized intervals were chosen within the minimum–maximum range across all groups. (**C**) The maximum difference between cumulative distributions shown in **B** (KS–S) for all group comparisons. *Right*: Dots highlight the comparison in the PTX group versus all other groups. *Left*: Dots represent all other comparisons. Significant data are denoted with asterisks: $^{*}P < 0.05$; $^{**}P < 0.01$; $^{***}P < 0.001$.

Blockage of STAT-3 restores neuronal firing under epileptogenic conditions

We first focused on single-neuron dynamics, and in each neuron, we calculated the instantaneous frequency of calcium events (IF, i.e. the inverse of the time interval between consecutive calcium spikes) as an indicator of neural firing frequency and general circuit excitability. The effective need of a prolonged exposure (3 days) to GABAergic synaptic blockers to affect neural firing was preliminarily verified. The application of PTX just for 1 day slightly increased the average neural firing frequency compared to control conditions (0.06 and 0.04 Hz in PTX and in control conditions, respectively; Supplementary Fig. 1A). However, 3 days of PTX exposure significantly increased the average neural firing frequency 3-fold compared to 1 day of PTX exposure at 0.18 Hz (Supplementary Fig. 1B). To further confirm our model, we imaged the slices in the presence of PTX (on the third day of exposure) and also at 3D (i.e. 3 days after the PTX wash out). The hyper-excitable epileptic-like state in presence of PTX was characterized by an average neural firing frequency of 0.15 Hz: significantly higher than the corresponding control condition. Therefore, the average neural firing frequency was significantly increased compared to corresponding baseline conditions both in presence of PTX and similarly 3 days after the wash out of PTX (Supplementary Fig. 1C). Baseline control activity and hyper-active neural firing observed in PTX-treated slices at 3D was abolished in presence of glutamatergic synaptic blockers (CNQX 20 µM and D-AP5 10 µM blocking AMPA/Kainate and NMDA receptors, respectively), confirming that baseline activity and higher neural firing induced by long PTX exposure are grounded on glutamatergic transmission (Supplementary Fig. 1D). Given these observations, we used 3 days of PTX treatment to have a clear impact after the wash out of the GABAergic blocker.

We next focused on single-neuron dynamics under the four different experimental conditions at 3D, 7D and 10D (Fig. 2) after PTX exposure. We imaged an average of 98 ± 22 neurons across all experimental conditions as summarized in Table 1, on a total of $n =$

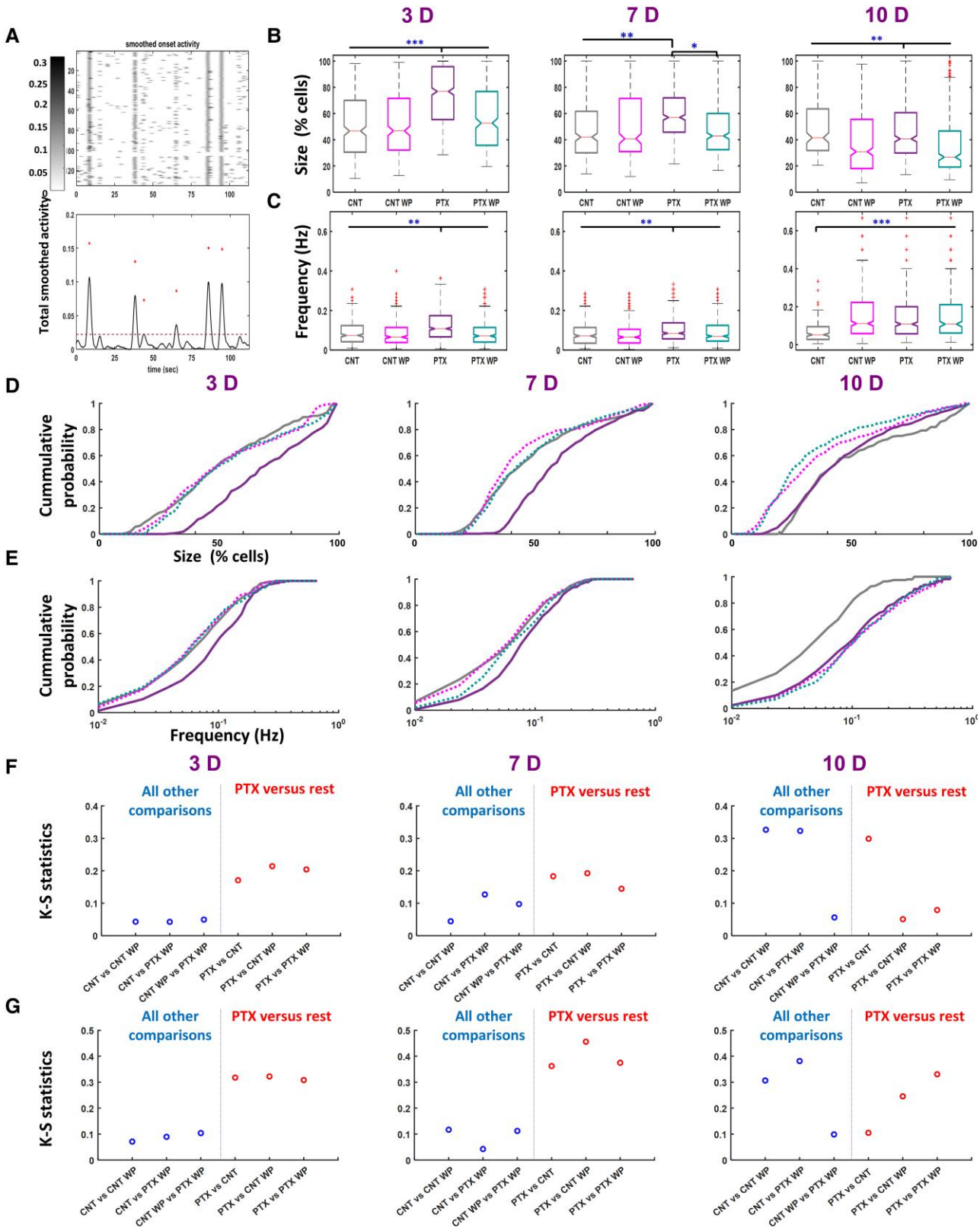

Figure 4 Ensemble level: size and frequency of circuits' synchronizations. (**A**) Representative zoomed raster plot (*top*) of the smoothed calcium spike onsets and the sum per frame of the activity (*bottom*). The asterisks mark synchronizations for which the sizes were above chance level (marked as a horizontal line). (**B** and **C**) Pooled values of synchronization sizes (**B**) and frequencies (**C**) at 3–7 and 10D across all slices showing median (horizontal line) 25th–75th percentile limits, bottom–top range values and outliers (marked by red asterisks). (**D** and **E**) Cumulative distributions of synchronization sizes (**D**) and frequencies (**E**) obtained as averages across slices belonging to the same conditions. Fifty identical equally sized intervals were chosen within the minimum–maximum range across all groups. (**F** and **G**) Maximum differences (KS–S) between cumulative distributions shown in **D** and **E**, respectively, for all group comparisons. *Right*: Dots highlight the comparison in the PTX group versus all other groups. *Left*: Dots represent all other comparisons. Significant data are denoted with asterisks. *$P < 0.05$; **$P < 0.01$; ***$P < 0.001$. A similar plot scheme to Figs 2 and 3 was used in **B**–**G**.

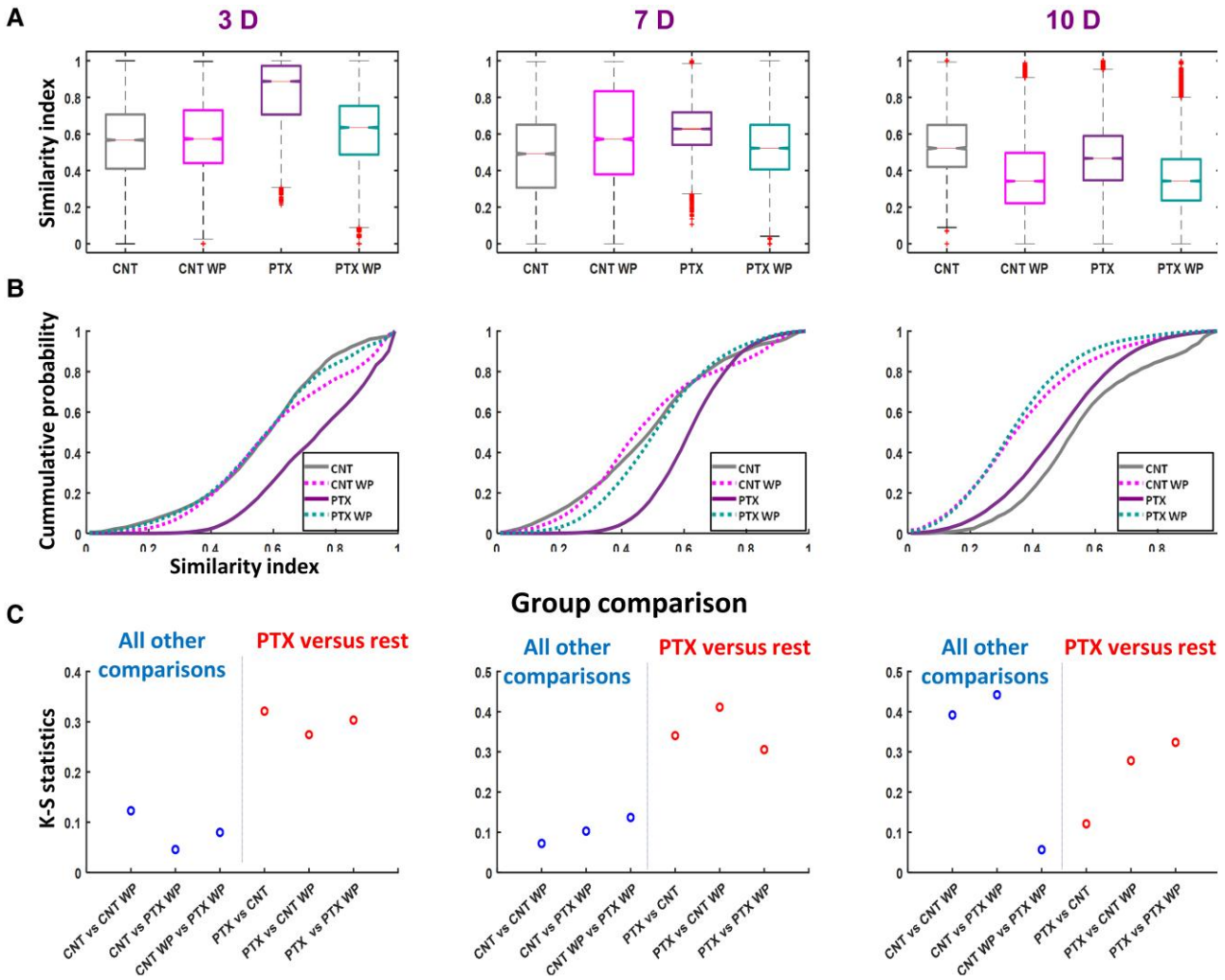

Figure 5 Ensemble level: similarity between circuits' synchronizations. (**A**) Pooled values at 3–7 and 10D across all slices show the median (horizontal line) 25th–75th percentile limits, bottom to top range values and outliers (marked by red asterisks). (**B**) Cumulative distributions obtained as averages across slices belonging to the same conditions. Fifty identical equally sized intervals were chosen within the minimum–maximum range across all groups. (**C**) Maximum difference between cumulative distributions shown in **B** (KS–S) for all group comparisons. *Right*: Dots highlight the comparison in the PTX group versus all other groups. *Left*: Dots represent all other comparisons. A similar plot scheme to Figs 2 and 3 was used.

60 slices. The comparison of single-neuron firing frequency between groups (and similarly to other neural dynamics variables shown in Figs 3, 4 and 5) was performed both on the values of IF pooled across all slices and neurons (obtaining one global distribution per group; Fig. 2A) and on the average cumulative distributions of IF across slices (Fig. 2B and C), as described below.

After pooling IFs across all neurons from all slices within the same group and day of recording ($n \geq 325$, see Table 1), non-parametric group comparison (Kruskal–Wallis test, see 'Materials and methods' section) revealed a significant difference at 3D, 7D and 10D between the PTX group and all other groups (Fig. 2A). Although differences in some cases could also be detected between other groups, the median IF of the PTX group (Fig. 2A, red horizontal line in the bar plots) was always the highest.

Further quantification of the statistical difference between the groups was performed using the distance between average cumulative distributions (in this case data were not pooled but averaged across slices, and therefore a representative average cumulative distribution for each group and recording day was reconstructed; see 'Materials and methods' section and Fig. 2B). We used the KS-S, i.e. the maximum difference between cumulative distributions (Fig. 2C), as a metric of distance (i.e. difference) between groups. The KS-S values between the epileptic group (PTX) and all other groups (CNT, PTX-WP and CNT-WP; see red dots in Fig. 2C) were always (i.e. at 3D, 7D and 10D) higher when compared to the distance between the other groups (blue dots).

Summarizing the results, the higher levels of single-neuron firing in the circuits exposed to epileptogenic conditions (PTX group) confirmed the induction of a hyper-excitable epileptic-like state. Importantly, the acute inhibition of the STAT3 restored the level of single-neuron firing to baseline control conditions.

Blockage of STAT3 preserve physiological neuronal pair-wise dynamics

As ictal and inter-ictal epileptic dynamics are characterized by pathological synchronous events across neurons and brain circuits, we next looked at the coordinated firing across cells in the circuits, focusing first on the neuronal pairs level. Physiologically, communication between neuronal pairs leads to correlated neuronal pair

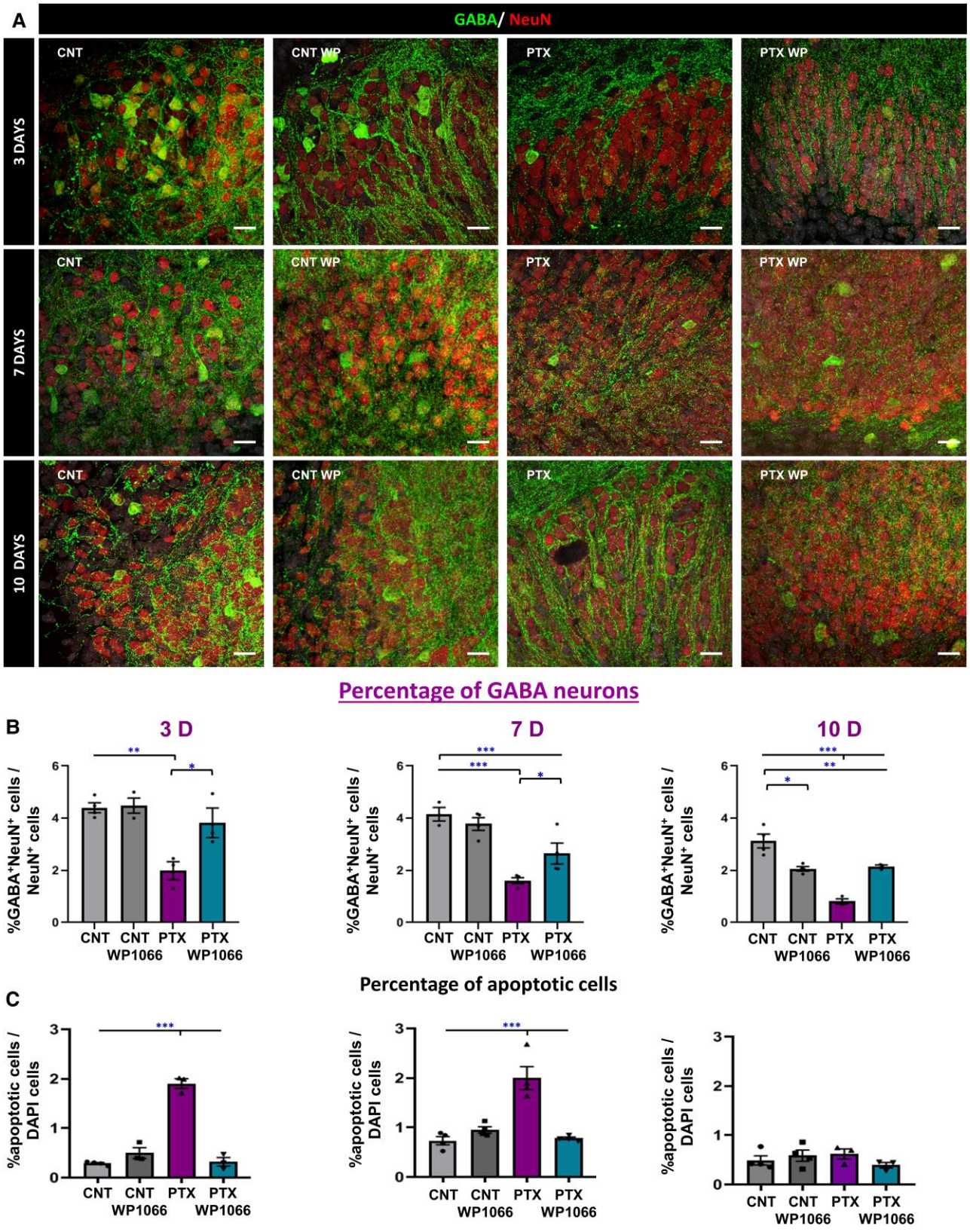

Figure 6 Characterization of circuit composition through GABAergic and apoptotic cell density: WP1066 prevents cell loss and death of GABAergic neurons. (**A**) Representative confocal microscopy images showing GABA-positive cells in the granule cell layer under the different conditions at 3, 7 and 10 days. (**B**) Quantification of the proportion of GABA/NeuN-positive cells among the total number of NeuN-positive cells at 3, 7 and 10 days after the addition of PTX/WP1066. (**C**) Quantification of the proportion of apoptotic cells in the slices at 3, 7 and 10 days after the addition of PTX/WP1066. Scale bar = 10 μm. One-way ANOVA after all pair-wise multiple comparisons by the Holm–Sidak *post hoc* test. Bars show mean ± SEM. Dots show individual data. $^{*}P < 0.05$, $^{**}P < 0.01$, $^{***}P < 0.001$.

activity. However, synchronous epileptic dynamics could emerge from the pair-wise level scaling up to circuits. Therefore, we expected a higher pair-wise correlation in the spontaneous firing of epileptic circuits. As a result, we calculated the correlation between the smoothed time series of neuronal firing (see Fig. 3 and 'Materials and methods' section).

Non-parametric group comparison of the pooled statistics of firing correlations across all neuronal pairs and slices showed significant differences between all groups at 3D, 7D and 10D (Fig. 3A). Note that the statistic on the neuronal pair scales was the square of the number of neurons; therefore, the number of pooled observations in each group and on each recording day was very high (>17 530 neuronal pairs) compared to single-neuron statistics. At 3D, the median of the firing correlations in the PTX group was remarkably higher (>33%) when compared to the other cases (0.52 in PTX, 0.39 in CNT, 0.23 CNT-WP and 0.34 in PTX-WP group, respectively). Also, on 3D the KS-S revealed higher differences between the epileptic group and other groups as shown in Fig. 3B and C. The same trend, but attenuated, was observed at 7D with higher pair correlation (>11%; 0.30 PTX, 0.22 CNT, 0.18 CNT-WP, 0.27 PTX-WP group) and higher KS-S, when comparing the PTX group with the others. At 10D, both medians of IF and KS-S differences showed similar values when comparing groups. Summarizing the results, higher levels of pair-wise synchronized dynamics were observed in the epileptic group at 3D and 7D, but not at 10D (when also the density of alive cells in the circuits displayed lowest values, as previously shown in Fig. 1E).

Blockage of STAT3 restores neuronal ensemble synchronization

Since synchronization is a key feature of epileptic activity, but also a physiological feature of spontaneous circuit dynamics, we next quantified NS (Fig. 4). Because synchronized events could also be detected by chance, simply as a consequence of the background neuronal activity, we considered only synchronizations with a number of recruited cells above chance level (Fig. 4A) here; these were estimated from reshuffled random firings keeping the same firing frequency in a single neuron (see the 'Materials and methods' section). Similar to the single-neuron firing, we first verified that a prolonged exposure (3 days) to GABAergic synaptic blockers endured a sufficiently long epileptogenic time window to impact NS (Supplementary Fig. 2). When looking at the frequency of circuit synchronization for slices treated for only 1 day with PTX, we did not observe any significant increase in the frequency of circuit synchronizations compared to corresponding control conditions (Supplementary Fig. 2A). On the contrary, a significant increase in the synchronization frequency was observed when slices were treated for 3 days with PTX (Supplementary Fig. 2B). Notably, a similar increase in the frequency of synchronizations was observed in the presence of PTX (i.e. the disinhibited epileptic condition; Supplementary Fig. 2C).

Next, we quantified the instantaneous frequency (Fig. 4B, D and F) and the size (Fig. 4C, E and G) of the synchronizations; the latter was quantified as a percentage of recruited cells within the imaged neural population.

The pooled statistics of circuits' synchronizations showed similar trends at 3D and 7D. Specifically, non-parametric statistics showed that the PTX groups were significantly different from all other groups in terms of frequency and size of circuit synchronization ($P < 0.05$), whereas all other groups did not show significant differences between them. Higher frequencies of synchronizations (medians at 3D and 7D of PTX group were 0.11 and 0.09 Hz, respectively, while all other groups had median values of 0.07 Hz) and percentage of recruited neurons in synchronized events (medians of groups at 3D: PTX 76.8%, CNT 46.6%, CNT-WP 46.8%, PTX-WP 52.7%; medians of groups at 7D: PTX 57%, CNT 42.0%, CNT-WP 40.8%, PTX-WP 42.9%) were observed in the PTX group compared to the other groups. Similarly, at 3D and 7D, the KS-S showed higher differences between the PTX group and all other groups (Fig. 4B and C). At 10D, such trends were no longer observed and the pooled statistics revealed a significant difference between CNT and all other groups in terms of synchronization frequency (Fig. 4C); whereas, in terms of synchronization size, all groups were significantly different apart from the cases of CNT versus PTX and CNT-WP versus PTX-WP (Fig. 4D). At 10D, the KS-S did not show the previous trends observed at 3D and 7D. Summarizing the results, synchronized ensemble dynamics in the epileptic group were more frequent and recruited a larger number of neurons at 3D and 7D, whereas at 10D such trends did not persist.

Given that epileptic circuits present dysfunctional topological organizations with hypersynchronous patterns, to characterize the complexity of spontaneous ensemble dynamics in terms of the richness in the repertoire of synchronization patterns generated by the circuits, we observed similarity between the circuit synchronizations (Fig. 5). The underlying hypothesis was that, in a dysfunctional circuit, reduced complexity should be observed in the generated patterns and dynamics. We quantified the similarity of the generated synchronized patterns as the cosine of the angle between the binary vectors representing the neurons recruited in the circuit synchronizations (see the 'Materials and methods' section). The pooled statistics revealed significant differences between all groups at 3D, 7D and 10D (Fig. 5A). Note that in this case, as in the neuronal pairs correlation, the number of observations (>3008 pairs of synchronization) scaled as the square of the total number of synchronizations. At 3D, the median similarity of the synchronizations generated in the PTX group was very high (median 0.89 out of a possible maximum of 1) compared to the other groups (0.57 CNT, 0.57 CNT-WP and 0.64 PTX-WP). The gap was attenuated at 7D (0.63 PTX, 0.49 CNT, 0.57 CNT-WP and 0.52 PTX-WP). KS-S showed clearly how the distribution of events both at 3D and 7D in the PTX group was consistently more distant to all other groups (Fig. 5B and C). These trends in the similarity of synchronization patterns were not present at 10D.

Blockage of STAT3 prevents gliosis and loss of GABAergic cells in epileptogenic conditions

The PTX group showed stereotypical patterns of hyper-excitable epileptic states from single-neuron firing to increased pair-wise correlations and larger ensemble synchronizations. These alterations were attenuated in general by the inhibition of STAT3. We therefore tested whether this beneficial effect could be mediated by a reduction in neuroinflammation and preservation of interneurons (i.e. GABAergic neurons). We first performed immunostaining to quantify the density of apoptotic cells and of inhibitory neurons (i.e. GABAergic cells). According to previous reports[28–30] on the loss of GABAergic neurons across the development and instalment of epilepsy, we hypothesized that: (i) PTX induces the loss of GABA cells leading to hyper-excitable circuit states; and (ii) inhibition of STAT3 during the time window of epileptogenesis reduces cellular damage affecting the emergence of epileptic circuit dynamics (Figs 2–4).

As a result, we quantified the number of GABA-positive cells in the GCL, out of the whole population of neurons (NeuN-positive cells; Fig. 6A). At 3D, we saw that the presence of GABA cells in the epileptic group was reduced to 2%, ~50% less than that seen under all other conditions, in which the GABAergic population represented ~4% of the overall neural population (Fig. 6B). Similar results were obtained at 7D (central plot of Fig. 6B), although showing a general decrease in the GABAergic population under all conditions (more pronounced in the PTX-WP group with values around 3%). Also, at 10D we observed under all conditions a general decrease in the percentage of GABAergic neurons, but the trend for 3D and 7D to have the lowest values observed in the PTX group was maintained (right plots of Fig. 6B). We further confirmed these results by using GAD antibody (Supplementary Fig. 3A). The quantification of GAD-positive cells in the GCL across the different experimental conditions at 3D presented the same trend shown when using the GABA antibody, although with slightly lower density values (Supplementary Fig. 3B).

Since GABAergic cell presence was reduced under epileptic conditions but preserved by the acute blockage of the STAT3, we next looked at overall cell loss and quantified the presence of dead cells at 3, 7 and 10 days counting the number of apoptotic cells GCL + SGZ (see the 'Materials and methods' section) as a readout of cellular damage through nuclear staining using DAPI (Fig. 6C). We found that at 3D and 7D, cell loss was higher in the epileptic group, with a more significant ratio of apoptotic cells compared to the other conditions. This result highlighted general circuit structural damage in the epileptic group. The inhibition of STAT3 under epileptogenesis (PTX-WP group) prevented general cellular damage. At 10D, the whole experimental group showed a similar presence of dead cells, but this also corresponded to the lowest and similar densities of live cells in the cultures (as previously shown in Fig. 1E).

Overall, these immuno-characterizations showed that epileptic conditions induce a general loss of cells targeting the GABAergic neuronal population preferentially, which was decreased to half of the baseline levels, and that anti-inflammatory conditions prevent overall cell loss, specifically that of GABAergic cells.

Since we studied the impact on the epileptogenic conditions of inhibiting the STAT3-mediated response, we next characterized the inflammatory profile of the circuit in the different glial populations. Reactive glia, involving both astrocytes and microglia, is one of the hallmarks of epilepsy. We first focused on reactive astrogliosis, measuring the overall area occupied by GFAP staining at 3D, 7D and 10D, because an overexpression of GFAP represents a hallmark of reactive astrocytes (Fig. 7A). At 3D, 7D and 10D, the expression of GFAP was significantly higher in the PTX group compared to all other groups (Fig. 7B). However, the inhibition of STAT3 significantly reduced the area occupied by GFAP to control levels.

Next, we tested the reactivity of the microglia cells, using the specific microglial marker Iba1 (Fig. 7C). Similar to what we observed for astrocytes, we found that the expression of Iba1, as measured by the area occupied by the marker, was significantly increased in the PTX group compared to all other groups at 3D, 7D and 10D (Fig. 7D). The blockage of STAT3 reduced the area occupied by Iba1 to control levels.

Our results on glial reactivity show that STAT3 transcription inhibition alone was able to prevent the reactivity response of both astrocytes and microglial cells under epileptogenic conditions.

The overall immunostaining characterizations of the structural and inflammatory profiles of the circuits show that hyper-excitable conditions induce a general reactive gliosis accompanied by an increase in the number of apoptotic cells with a greater loss in GABAergic population, which are stereotypical hallmarks of epileptic states. Notably, we emphasize again that the sole inhibition of STA3 transcription was capable of preventing the induction of these epileptic markers.

Discussion

We used organotypic hippocampal cultures as an *in vitro* model of TLE, similar that described previously in the literature.[17,18,31] We exposed transitorily cultured circuits to pro-epileptic hyper-excitable conditions by suppressing GABAergic synaptic transmission to model epileptogenesis. Preliminarily, we report that prolonged exposure to GABAergic synaptic blocker PTX (3 days of treatment) was effective and needed to observe a clear impact on neural dynamics. This effect was not achieved when the slices were exposed to PTX for just 1 day. Using calcium imaging to monitor spontaneous neural dynamics simultaneously in dozens of neurons from 3 to 10 days following epileptogenic episodes, we observed that at 3D and 7D monitored circuits showed increased single-neuron firing, increased firing correlations in neural pairs, higher frequencies of circuit synchronizations with higher numbers of recruited neurons and decreased complexity of synchronized patterns (i.e. a less rich repertoire of activity as reflected by a higher similarity between generated patterns). In addition, in agreement with previous results on epileptic circuits, we observed increased cellular loss,[27] particularly with respect to the GABAergic population.[29]

It is known that the pattern of expression of organization of GABAergic cells in developmental circuits resembling adult conditions was not observed before P10.[32,33] This is a key point to understanding the percentage of GABAergic cells obtained in our experimental model, as it is based on slices extracted at P5–7.

Therefore, a lower presence of inhibitory cells was present in the epileptic circuits, favouring the appearance of hyper-excitable states with an increased frequency of single-cell and coordinating circuit activity. Moreover, epileptic circuits showed a persistent inflammatory glial profile as revealed by astrocytic and microglial markers

Although such observations on *in vitro* hippocampal slices are in general agreement with previous literature,[31,34] to the best of our knowledge, this is the first time that spontaneous synchronizations and emergent collective dynamics have been studied consistently and quantified in epileptic circuits longitudinally over the days after epileptogenesis. This was made possible by maintaining undisturbed culture conditions during the imaging sessions, avoiding the perfusion of extracellular ACSF or medium, which was a major protocol used in previous works.[18]

When we selectively blocked STAT3,[35] concomitantly during the time windows of epileptogenesis (by simultaneous application of PTX and WP1066), we observed that epileptic dynamics, cellular loss, GABAergic cell depletion and reactive gliosis were not present in the neuro-glial circuits, with variable values at baseline control levels. This was clear longitudinally at 3 and 7 days following epileptogenesis, whereas at 10 days no clear differences or trends were observed.

The general loss of difference between the experimental conditions at 10D, in terms of circuit dynamics, GABAergic density and neuro-inflammatory profile, can be explained by the progressive cell loss and decreased density of alive cells in the cultured circuits, which occurred under control conditions and all other tested conditions. Although at 10D the level of apoptosis in all groups was similar, importantly, the composition of the neuronal population could

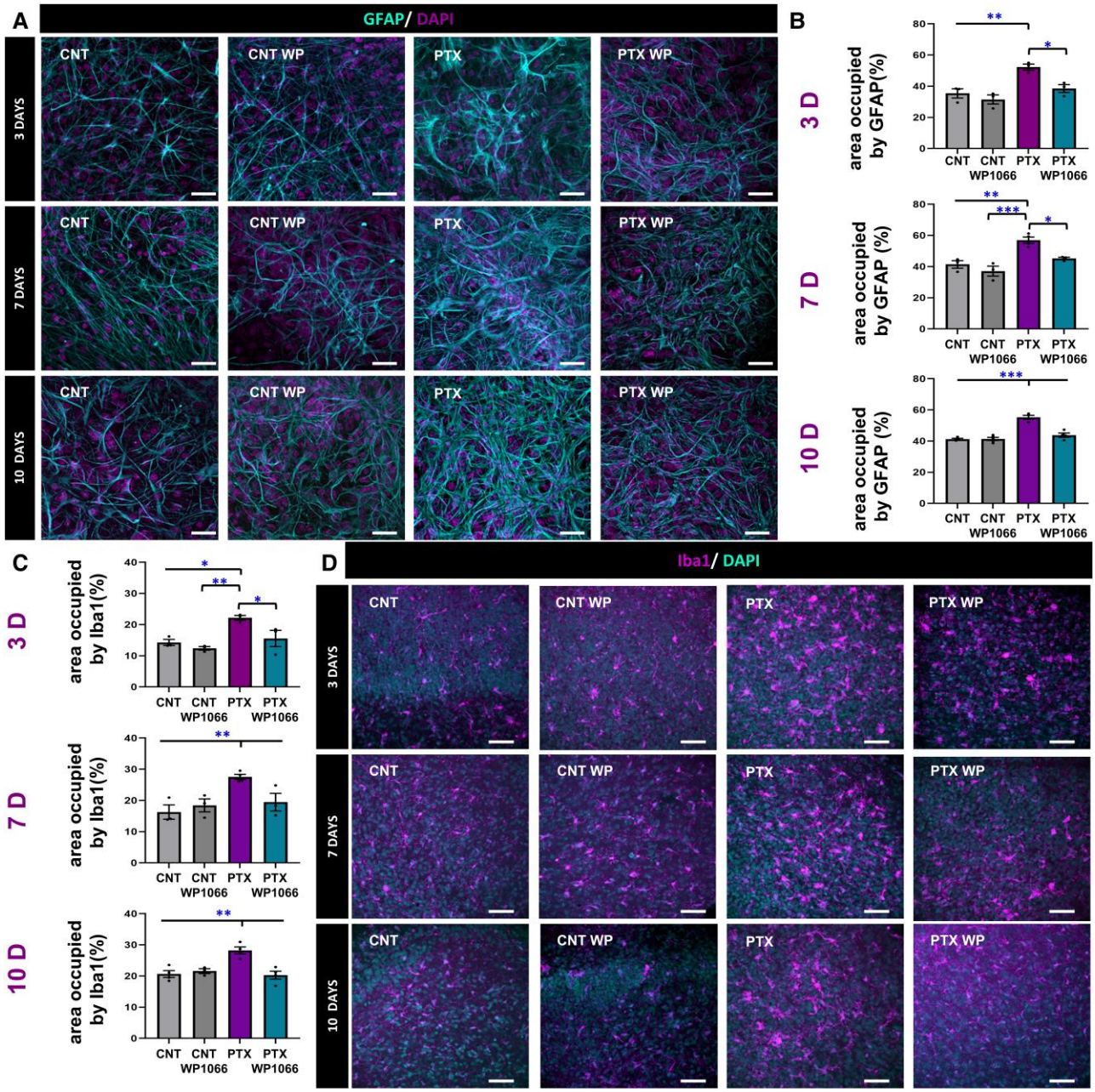

Figure 7 Circuits' neuro-inflammatory profile: WP1066 prevent the glial inflammatory state that is present in epileptic circuits. (**A**) Representative confocal microscopy images showing the area occupied by the astrocytic marker GFAP in the different conditions at 3, 7 and 10 days. (**B**) Quantification of the area occupied by GFAP at 3, 7 and 10 days after the addition of PTX/WP1066. (**C**) Quantification of area occupied by Iba1 at 3, 7 and 10 days after the addition of PTX/WP1066. (**D**) Representative confocal microscopy images showing the area occupied by the microglial marker Iba1 at 3, 7 and 10 days. Scale bar = 10 μm. One-way ANOVA after all pair-wise multiple comparisons by the Holm–Sidak *post hoc* test. Bars show mean ± SEM. Dots show individual data. $^{*}P < 0.05$, $^{**}P < 0.01$, $^{***}P < 0.001$.

play a role, since the GABAergic population was preserved with the treatment (WP1066).

It has been reported that time in culture directly affects the integrity and viability of cultured slices,[27] with the period from DIV7 to DIV14 being of particular vulnerability, and eventually the slices cannot be maintained alive past a few weeks. Organotypic hippocampal slices are commonly used as an *in vitro* model of seizures and chronic epilepsy.[17] Here, we demonstrated that PTX-treated organotypic cultures recapitulate the most typical features of epileptogenesis: spontaneous electrical seizures, cell death, inflammation and alteration of neuronal circuitry, as previously described by other authors.[31,34] Although there is some controversy about the intrinsic epileptic profile of organotypic slices, even under control conditions,[36] our results demonstrated that PTX-treated organotypic slices are an excellent model for studying and understanding epileptogenesis. Indeed, when we imaged slices under commonly used conditions, i.e. by perfusion of ACSF losing culture conditions, we did not observe spontaneous synchronizations (unshown).

Here we focused on the role of STAT3 in the development of epilepsy and neuroinflammation. The JAK/STAT3 pathway is known to be rapidly activated in the hippocampus after status epilepticus.[37] Previous reports have linked STAT3 activation to epileptogenesis,[38] suggesting that STAT3 remains activated for up to 1 month, maintaining and aggravating the effect of astrogliosis.[15] STAT3 could thus promote spontaneous seizures by contributing to reactive gliosis triggered by the initial event. STAT3 can be pharmacologically blocked by different drugs such as Pyridone or WP1066. It was shown that STAT3 blocked by WP1066 lowered the number of spontaneous seizures in a rat pilocarpine model of epilepsy reducing the severity of subsequent seizures.[16]

We herein extend some of these results, and show that inhibition of STAT3 with WP1066 not only reduced the effect of epilepsy on neuronal circuit functionality, but this strategy also precisely preserved the topology of the circuit. We show that the alteration of the neuronal circuits was accompanied by topological changes such as the loss of GABAergic cells. We observed that the number of GABAergic cells decreased in comparison to control conditions at all time points. Interestingly, this loss of GABAergic cells has been shown in *in vivo* TLE induced models by pilocarpine.[29] The role of GABAergic neurons in the development and prevalence of epilepsy has been extensively studied in animal models, demonstrating that GABAergic interneuron loss can change the excitation/inhibition balance. In this work, we have shown for the very first time that STAT3 blockage reduces GABAergic cell loss in an *in vitro* model of epilepsy.

Neuroinflammation is another hallmark of epilepsy; therefore, we resorted to analyse the inflammatory profile of the organotypic slices. Gliosis includes both reactive astrocytes and reactive microglia, as astrocytes and microglia are interconnected such that the activity of one cell type affects the activity of the other.[28,39–41] Here, gliosis was measured by the area occupied by astrocytes and microglia. Our results confirm previous results in which STAT3 inhibition reduced GFAP and Iba1 overexpression after epilepsy.[15] Thus, we have shown that STAT3 inhibition could affect the activation of astrocytes and microglia in the epileptogenic process.

Our data suggest that the JAK/STAT inhibition at the onset of the epileptic event could modify the progress of epilepsy. Inhibition of this pathway may open up novel therapeutic possibilities as a complement to other commonly used anticonvulsant drugs.

Acknowledgements

We thank Professor Juan Manuel Encinas for his comments and insights, and Javier Garcia Diez-Garcia for his help on microscopy and calcium imaging.

Funding

We acknowledge the financial support of FEDER (grant reference AI-2021-039), the Spanish Ministry for Science and Innovation (MICINN; grant reference PID2021-127163NB-I00, funded by the MCIN/AEI/10.13039/501100011033/FEDER, UE), and the Ikerbasque start-up funding. S.M.-S. received a Juan de la Cierva-formación Fellowship (FJC2018-035496-I) and later a HPC&Ai-IKUR (funded by the Basque Government) Postdoctoral Fellowship.

Competing interests

The authors report no competing interests.

Supplementary material

Supplementary material is available at *Brain* online.

References

1. Covolan L, Mello LE. Temporal profile of neuronal injury following pilocarpine or kainic acid-induced status epilepticus. *Epilepsy Res*. 2000;39:133-152.
2. Curia G, Longo D, Biagini G, Jones RSG, Avoli M. The pilocarpine model of temporal lobe epilepsy. *J Neurosci Methods*. 2008;172:143-157.
3. Fujikawa DG. The temporal evolution of neuronal damage from pilocarpine-induced status epilepticus. *Brain Res*. 1996;725:11-22.
4. Lévesque M, Avoli M, Bernard C. Animal models of temporal lobe epilepsy following systemic chemoconvulsant administration. *J Neurosci Methods*. 2016;260:45-52.
5. Stephen LJ, Kwan P, Brodie MJ. Does the cause of localisation-related epilepsy influence the response to antiepileptic drug treatment? *Epilepsia*. 2001;42:357-362.
6. Duncan JS, Sander JW, Sisodiya SM, Walker MC. Adult epilepsy. *Lancet*. 2006;367:1087-1100.
7. Brodie MJ, Barry SJE, Bamagous GA, Norrie JD, Kwan P. Patterns of treatment response in newly diagnosed epilepsy. *Neurology*. 2012;78:1548-1554.
8. Macdonald RL, Kelly KM. Antiepileptic drug mechanisms of action. *Epilepsia*. 1995;36(s2):S2-S12.
9. Rogawski MA, Löscher W, Rho JM. Mechanisms of action of antiseizure drugs and the ketogenic diet. *Cold Spring Harb Perspect Med*. 2016;6:a022780.
10. Vezzani A, French J, Bartfai T, Baram TZ. The role of inflammation in epilepsy. *Nat Rev Neurol*. 2011;7:31-40.
11. Quirico-Santos T, Meira ID, Gomes AC, *et al*. Resection of the epileptogenic lesion abolishes seizures and reduces inflammatory cytokines of patients with temporal lobe epilepsy. *J Neuroimmunol*. 2013;254(1–2):125-130.
12. Ghoreschi K, Jesson MI, Li X, *et al*. Modulation of innate and adaptive immune responses by tofacitinib (CP-690,550). *J Immunol Baltim Md 1950*. 2011;186:4234-4243.
13. Nicolas CS, Peineau S, Amici M, *et al*. The Jak/STAT pathway is involved in synaptic plasticity. *Neuron*. 2012;73:374-390.
14. Nicolas CS, Amici M, Bortolotto ZA, *et al*. The role of JAK-STAT signaling within the CNS. *JAKSTAT*. 2013;2:e22925.
15. Xu Z, Xue T, Zhang Z, *et al*. Role of signal transducer and activator of transcription-3 in up-regulation of GFAP after epilepsy. *Neurochem Res*. 2011;36:2208-2215.
16. Grabenstatter HL, Angel YCD, Carlsen J, *et al*. The effect of STAT3 inhibition on status epilepticus and subsequent spontaneous seizures in the pilocarpine model of acquired epilepsy. *Neurobiol Dis*. 2014;62:73-85.
17. Abiega O, Beccari S, Diaz-Aparicio I, *et al*. Neuronal hyperactivity disturbs ATP microgradients, impairs microglial motility, and reduces phagocytic receptor expression triggering apoptosis/microglial phagocytosis uncoupling. *PLoS Biol*. 2016;14:e1002466.
18. Stoppini L, Buchs PA, Muller D. A simple method for organotypic cultures of nervous tissue. *J Neurosci Methods*. 1991;37:173-182.
19. Cronberg T, Rytter A, Asztély F, Söder A, Wieloch T. Glucose but not lactate in combination with acidosis aggravates ischemic neuronal death *in vitro*. *Stroke*. 2004;35:753-757.
20. Dana H, Sun Y, Mohar B, *et al*. High-performance calcium sensors for imaging activity in neuronal populations and microcompartments. *Nat Methods*. 2019;16:649-657.

21. Kanner S, Goldin M, Galron R, Ben Jacob E, Bonifazi P, Barzilai A. Astrocytes restore connectivity and synchronization in dysfunctional cerebellar networks. *Proc Natl Acad Sci U S A*. 2018; 115:8025-8030.
22. Friedrich J, Zhou P, Paninski L. Fast online deconvolution of calcium imaging data. *PLoS Comput Biol*. 2017;13:e1005423.
23. Encinas JM, Enikolopov G. Identifying and quantitating neural stem and progenitor cells in the adult brain. *Methods Cell Biol*. 2008;85:243-272.
24. Encinas JM, Michurina TV, Peunova N, *et al*. Division-coupled astrocytic differentiation and age-related depletion of neural stem cells in the adult hippocampus. *Cell Stem Cell*. 2011;8:566-579.
25. Martín-Suárez S, Abiega O, Ricobaraza A, Hernandez-Alcoceba R, Encinas JM. Alterations of the hippocampal neurogenic niche in a mouse model of Dravet syndrome. *Front Cell Dev Biol*. 2020;8:654.
26. Smirnov NV. Estimate of deviation between empirical distribution functions in two independent samples. (Russian). Bull. Moscow Univ. 1939:2(2);3–16.
27. Li F, Song Y, Dryer A, Cogguillo W, Berdichevsky Y, Zhou C. Nondestructive evaluation of progressive neuronal changes in organotypic rat hippocampal slice cultures using ultrahigh-resolution optical coherence microscopy. *Neurophotonics*. 2014; 1:025002.
28. Ben-Ari Y, Represa A. Brief seizure episodes induce long-term potentiation and mossy fibre sprouting in the hippocampus. *Trends Neurosci*. 1990;13:312-318.
29. Knopp A, Frahm C, Fidzinski P, Witte OW, Behr J. Loss of GABAergic neurons in the subiculum and its functional implications in temporal lobe epilepsy. *Brain*. 2008;131:1516-1527.
30. Houser CR. Do structural changes in GABA neurons give rise to the epileptic state? *Adv Exp Med Biol*. 2014;813:151-160.
31. Stoppini L, Duport S, Corrèges P. A new extracellular multirecording system for electrophysiological studies: application to hippocampal organotypic cultures. *J Neurosci Methods*. 1997;72: 23-33.
32. Ben-Ari Y, Rovira C, Gaiarsa JL, Corradetti R, Robain O, Cherubini E. Chapter 23: GABAergic mechanisms in the CA3 hippocampal region during early postnatal life. *Prog Brain Res*. 1990;83: 313-321.
33. Rozenberg F, Robain O, Jardin L, Ben-Ari Y. Distribution of GABAergic neurons in late fetal and early postnatal rat hippocampus. *Dev Brain Res*. 1989;50:177-187.
34. Duport S, Stoppini L, Corrèges P. Electrophysiological approach of the antiepileptic effect of dexamethasome on hippocampal slice culture using a multirecording system: the physiocard®. *Life Sci*. 1997;60:PL251-PL256.
35. Iwamaru A, Szymanski S, Iwado E, *et al*. A novel inhibitor of the STAT3 pathway induces apoptosis in malignant glioma cells both *in vitro* and *in vivo*. *Oncogene*. 2007;26:2435-2444.
36. Liu J, Saponjian Y, Mahoney MM, Staley KJ, Berdichevsky Y. Epileptogenesis in organotypic hippocampal cultures has limited dependence on culture medium composition. *PLoS One*. 2017;12:e0172677.
37. Raible DJ, Frey LC, Brooks-Kayal AR. Effects of JAK2-STAT3 signaling after cerebral insults. *JAKSTAT*. 2014;3:e29510.
38. Okamoto OK, Janjoppi L, Bonone FM, *et al*. Whole transcriptome analysis of the hippocampus: toward a molecular portrait of epileptogenesis. *BMC Genomics*. 2010;11:230.
39. Sanz P, Garcia-Gimeno MA. Reactive Glia inflammatory signaling pathways and epilepsy. *Int J Mol Sci*. 2020;21:4096.
40. Cohen I, Navarro V, Clemenceau S, Baulac M, Miles R. On the origin of interictal activity in human temporal lobe epilepsy *in vitro*. *Science*. 2002;298:1418-1421.
41. Knopp A, Kivi A, Wozny C, Heinemann U, Behr J. Cellular and network properties of the subiculum in the pilocarpine model of temporal lobe epilepsy. *J Comp Neurol*. 2005;483:476-488.